

Improving reservoir rock classification in heterogeneous carbonates using boosting and bagging strategies: A case study of early Triassic carbonates of coastal Fars, south Iran

J. Ghiasi-Freez^{1*}, M. Ziaii¹ and A. Moradzadeh²

1. Faculty of Mining, Petroleum & Geophysics Engineering, Shahrood University of Technology, Shahrood, Iran
2. School of Mining Engineering, College of Engineering, University of Tehran, Tehran, Iran

Received 27 January 2018; received in revised form 12 May 2018; accepted 14 May 2018

*Corresponding author: javadghiasi86@gmail.com (J. Ghiasi-Freez).

Abstract

An accurate reservoir characterization is a crucial task for the development of quantitative geological models and reservoir simulation. In the present research work, a novel view is presented on the reservoir characterization using the advantages of thin section image analysis and intelligent classification algorithms. The proposed methodology comprises three main steps. First, four classes of reservoir intervals are defined using a limited number of porosity and permeability values obtained from the core plugs of Kangan and Dalan formations. Then seven micro-scale features including distribution of pore types (interparticle, interaparticle, moldic, and vuggy), pore complexity, and cement distribution as well as textural characteristics are extracted from thin section images. Finally, the features extracted from each photomicrograph and its corresponding reservoir class are used as the training data for several intelligent classifiers including decision trees, discriminant analysis functions, support vector machines, K-nearest neighbor models and two ensemble algorithms, named bagging and boosting. The relationship between the micro-scale features and the reservoir classes was studied. Performance of all classifiers is evaluated using the concepts of accuracy, precision, recall, and harmonic average. The results obtained showed that the bagging decision tree delivered the best performance among the models and improved the accuracy of simple models up to 7.7% compared with the best single classifier.

Keywords: *Reservoir Characterization, Intelligent Classifiers, Boosting and Bagging Strategies, Image Analysis of Thin Sections, Kangan and Dalan Formations.*

1. Introduction

Reservoir characterization and identification of reservoir quality are the first prerequisites of petroleum recovery. The ideal state of a reservoir rock is not always true, especially in heterogeneous carbonate rocks. In spite of high porosity, various diagenesis processes and textural characteristics might dramatically reduce the permeability of carbonates. It is necessary to consider all these parameters simultaneously for a reliable reservoir characterization, which is possible throughout the advantages of data mining approaches. The present research work focuses on the advantages of thin sections prepared from core plugs to characterize heterogeneous carbonates.

Integrating the capabilities of image analysis and data mining approaches introduces an alternative approach, which can classify reservoir intervals based on the results of petrography, pore geometry, pore complexity, and pore type distribution. Data mining, intelligent classifier and pattern recognition models have found their place in petroleum engineering for reservoir characterization and rock typing. Estimation of missing logs or parts of incomplete log suites was the first application of the back-propagation neural network [1]. The primary implementations of neural network, fuzzy logic, and neuro-fuzzy have proven the potentials of the models for

developing a relationship between the log data and the core laboratory measurement [2-10]. Recently, the singular expert systems have integrated through the advantages of evolutionary algorithms, and the hybrid intelligent methodologies have been proposed for permeability prediction and reservoir characterization [11-16]. In addition, fast and accurate intelligent-based shortcuts have been proposed in order to solve various issues of petroleum engineering including prediction of over-pressurized zones (Cranganu [17]), classification of rock masses (Aydin [18]), characterization of naturally fractured zones (El Ouahed et al. [19]), rock facies classification (Dubois et al. [20]), incipient mechanical fault detection (Hu et al. [21]), water saturation and fluid distribution evaluation (Al-Bulushi et al. [22]), the z-factor estimation for natural hydrocarbon gases (Kamyab et al. [23]), prediction of CO₂ permeability of bituminous coal (Sharma et al. [24]), estimation of total and free fluid porosity from seismic attributes (Hatampour et al. [25]), and determination of the bubble point pressure (Elkatatny and Mahmoud [26]). A glance view on the literature shows that most of the previous research works have focused on the estimation and prediction tasks, while there are various intelligent classifiers available that can be used to find a precise evaluation of the reservoir rock properties. Moreover, foundation of the literature is based upon well log data, and the advantages of thin section images have been ignored. The main goal of the present research work was the improvement of reservoir rock characterization using various classification algorithms including single and integrated (bagging and boosting) strategies. A real case study from Kangan and Dalan formations was studied to verify the performance of the proposed approach. The novelty of this research work can be categorized into four parts. First, the advantage of thin section image analysis was employed for extracting the pore geometry and evaluating the pore shape complexity. Secondly, a quantitative petrography approach was introduced to measure the image features accurately. Thirdly, the performance of various classification algorithms was evaluated for permeability classification. Finally, an integrated fuzzy fusion of multi-classifiers was introduced to reap the advantages of all classifiers and cover the drawbacks of one model with another one.

2. Data preparation

The data necessary for this research work can be divided into two types: the core plug measurements and the image-based data that should be extracted from the thin section images. Fifty-six core samples each belonging to a different depth of Kangan and Dalan formations were available for the work. In the first step, three samples were prepared for each depth from the available rock samples of Kangan and Dalan formations. Two plugs were used for laboratory measurements of porosity and permeability, and the third one was for thin section preparation, which was saturated by blue epoxy dye in advance. The injected blue epoxy fills the porous media of the rock. The thin sections are prepared from the saturated samples, in which the pore spaces are easily distinguishable by the blue color. From the standpoint of sedimentology, the rare component of a rock can be naturally blue; due to this fact, all the blue spaces of the thin section can be considered as pore. Thin section images were captured under plane polarized light. The magnification was adjusted to 12.5X, in which both the texture and pore characteristics were clearly detectable. In the present work, first, the thin section images were processed using medial and low-pass filters to remove the possible noises and improve the image quality. Secondly, the color image was converted to a gray scale image to extract the cement distribution. In addition, the porous media of the images was extracted through an image binarization process to study the pore space geometry quantitatively.

3. Reservoir classification

Kangan and Dalan formations are the main reservoir rocks of South Pars Gas Field, the biggest gas accumulation in the world located in the southern borders of Iran. The Kangan and Dalan formations refer to Early Triassic and Late Permian, respectively. Limestone is the main lithology, while dolomite, anhydritic dolomite, and thin bed of shaly intervals have been recorded in the drilled wells from top to bottom of the formations. The limestone intervals of the Kangan and Dalan formations have been categorized as heterogeneous type, while several diagenetic processes affect the primary sediments. Figure 1 confirms that there is no exact relationship between the porosity and permeability in the limestones of the Kangan and Dalan formations, which is the evidence of diagenesis processes. It seems impossible to find a direct relationship between the porosity and permeability of the

samples due to their high heterogeneity. In order to solve this issue, the samples are classified into four types based on the porosity and permeability obtained in the laboratory according to the following description: class#1: Low porosity and low permeability; class#2: High porosity and low permeability; class#3: High porosity and fair permeability; class#4: high porosity and high permeability (Figure 2). Ten percent was the cut-off porosity value for division into the low and high categories. In addition, the following ranges

were used for low, fair, and high permeability: *low* (<10 mD), *fair* (10-100 mD), and *high* (>100 mD).

Table 1 represents the numerical porosity and permeability values for a limited number of core plugs measured in the laboratory. Although class#4 is the most desirable class from the standpoint of a petroleum geology for reservoir characterization, the frequency of its data is less than the other classes.

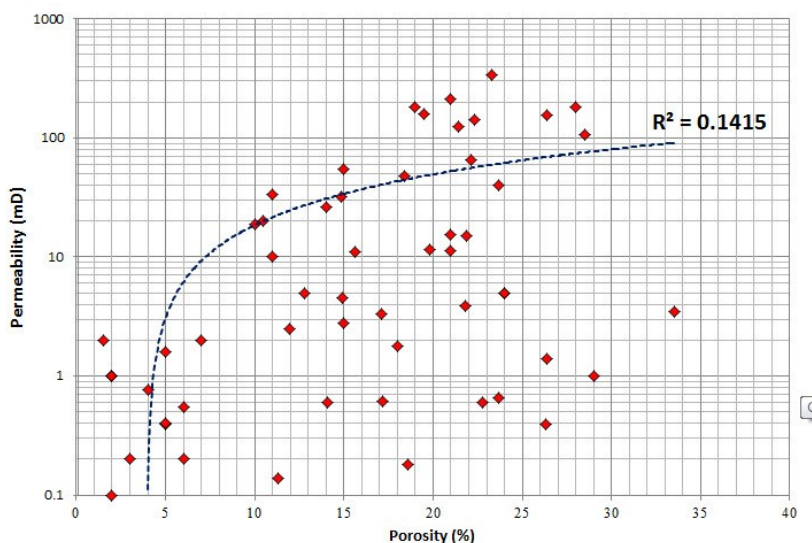


Figure 1. The cross-plot of core permeability versus porosity in the samples of Kangan and Dalan formations.

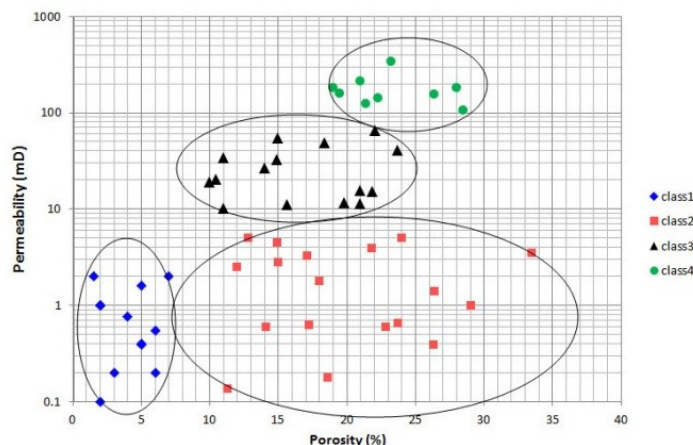


Figure 2. The defined classes of reservoir quality based on the porosity and permeability of the samples of Kangan and Dalan formations.

4. Feature extraction

In this section, the concepts and fundamentals of the extracted geometrical features, definition of pore complexity, criteria of cement points, and textural classification of the studied images are discussed in detail.

4.1. Pore geometry

The binary image was used to determine the size and geometrical characteristics of the pore spaces such as the perimeter, area, minor diameter, major diameter, equivalent diameter, roundness, elongation, anisotropy, solidity, and rectangularity (extent). Extraction of pore shape features is the prerequisite of pore type identification and calculating the abundance of various types of

porosity in the thin section image. The pore size measurement and pore geometry are readily accessible through point counting of the black objects of the binary images. Table 2 represents a brief introduction of these features. The geometrical parameters are determined for all the mesopores (50-100 μm) and macropores (>100 μm) of an image. The corresponding type of each pore space was obtained based on the extracted geometrical features through the pre-developed Matlab code for pore type identification, as discussed by Ghiasi-Freez et al. [27]. Then the areas of all pore spaces belonging to the same class were added together. The percentage of each type of porosity in the image was calculated by dividing the total area of that type by the total area of pore spaces larger than 50 μm. The percentages of porosity types including interparticle, interparticle, moldic (oomoldic and biomoldic), and vuggy in the images were

employed as inputs of the classifier models. Figure 3 compares the distribution of permeability versus the ratio of each type of pore space to the total optical porosity in the defined classes. The figures show that the porosity type and the amount of total optical porosity affect the permeability in parallel, which means that a high reservoir quality can be guaranteed by a highly effective optical porosity.

Figure 4 clarifies that the product of porosity type and total optical porosity is considered as a single parameter. Interparticle porosity is the only effective porosity type among the interparticle, moldic, and vuggy porosities. Large isolated molds and vugs entrap the fluid and reduce the fluid flow in the rock. Micro-porosity shows no relationship with permeability due to the lack of connection between pores and high percentage of micrite surrounding the micro-pores.

Table 1. Numerical values of core laboratory measurements for porosity and permeability of the studied samples.

#	Φ (%)	K (mD)	Class	#	Φ (%)	K (mD)	Class	#	Φ (%)	K (mD)	Class	#	Φ (%)	K (mD)	Class
1	5	1.6	1	15	26.4	1.4	2	29	24	5	2	43	10	19	3
2	5	0.39	1	16	26.3	0.39	2	30	24	5	2	44	23.7	40	3
3	7	2	1	17	11.28	0.137	2	31	17.1	3.3	2	45	22.1	65	3
4	6	0.55	1	18	11.96	2.49	2	32	33.5	3.5	2	46	15	54	3
5	1.98	1	1	19	14.9	4.5	2	33	19.84	11.5	3	47	18.4	48	3
6	1.98	1	1	20	22.8	0.6	2	34	21	11.2	3	48	23.2	340	4
7	4	0.76	1	21	23.7	0.65	2	35	15.65	11	3	49	21	213	4
8	2	1	1	22	18	1.8	2	36	11	10	3	50	28	181	4
9	6	0.2	1	23	18.58	0.18	2	37	14.01	26.18	3	51	19	180	4
10	2	0.1	1	24	12.8	5	2	38	21.88	15	3	52	19.5	158	4
11	5	0.4	1	25	14.1	0.6	2	39	14.88	32.13	3	53	28.5	105	4
12	1.5	2	1	26	17.2	0.62	2	40	10.5	20	3	54	21.4	123	4
13	3	0.2	1	27	21.8	3.9	2	41	11	33.5	3	55	26.4	155	4
14	29	1	2	28	15	2.8	2	42	21	15.5	3	56	22.3	142	4

Table 2. The geometrical features of pore spaces extracted from the binary images [27].

Geometrical feature	Mathematical formula
Roundness	$(\text{Perimeter})^2 / (4\pi \times \text{Area})$
Elongation	Major diameter/Minor diameter
Solidity	Area/Convex area
Eccentricity	Distance between foci of the ellipse/Major diameter
Rectangularity	Area/Bounding box area
Anisotropy	Equivalent diameter/Major diameter

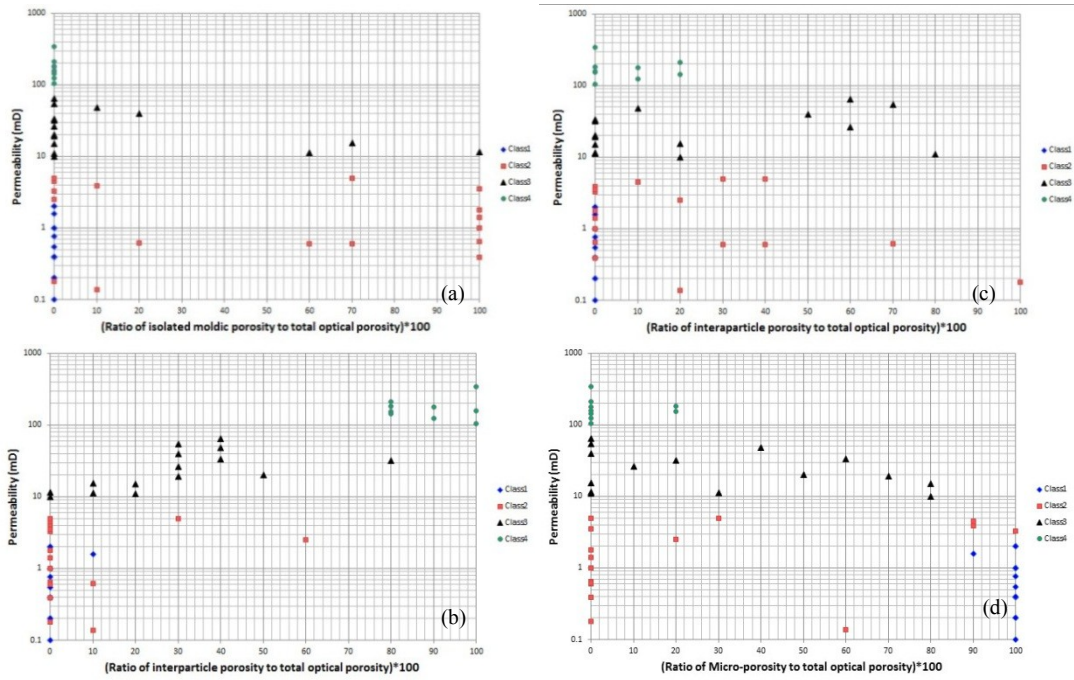


Figure 3. The distribution of permeability versus the ratio of (a) moldic, (b) interparticle, (c) interparticle, and (d) micro-porosity.

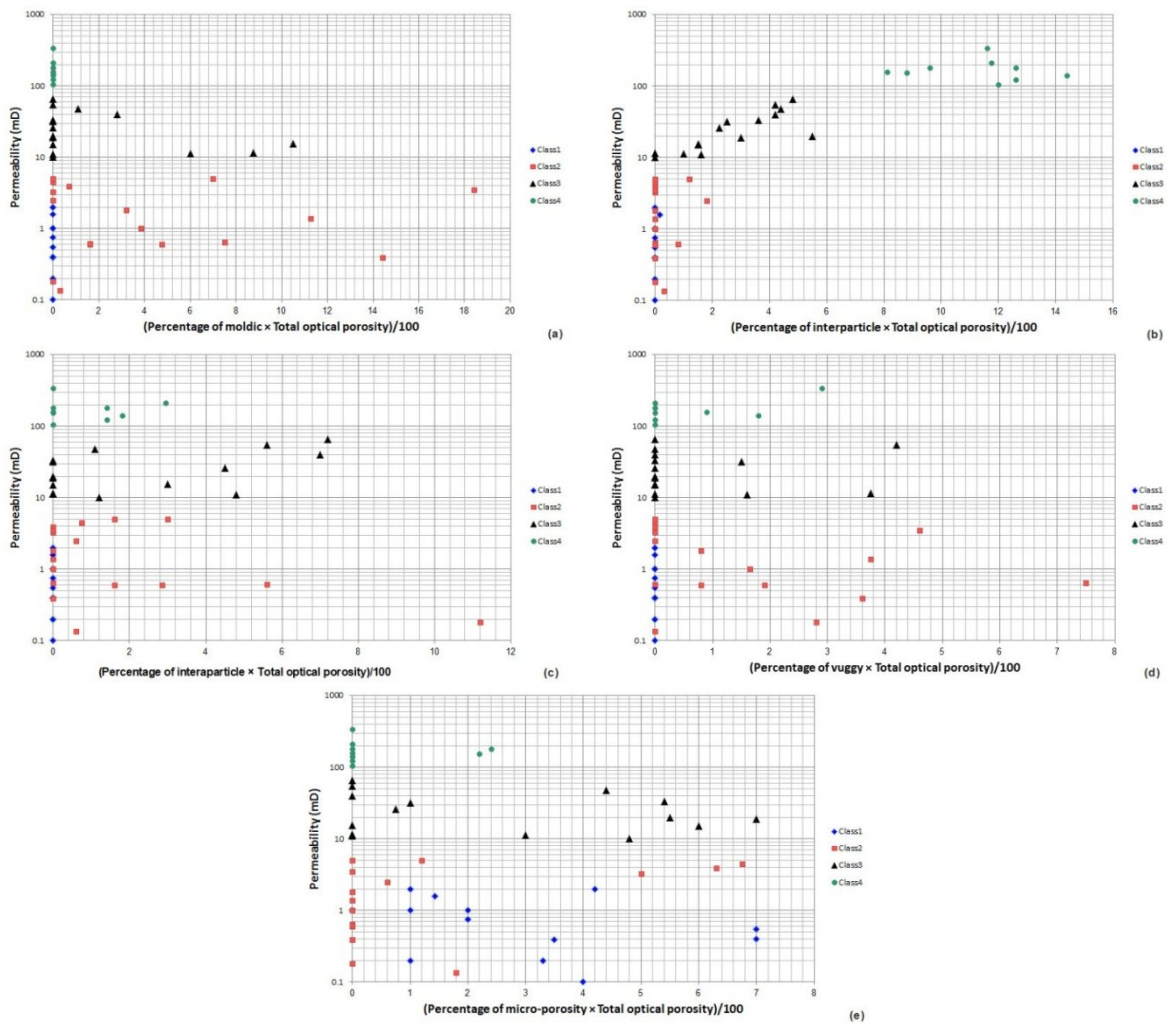


Figure 4. The relationship between permeability and the product of total porosity and (a) percentage of moldic porosity, (b) interparticle porosity, (c) interparticle porosity, (d) vuggy porosity and micro-porosity.

4.2. Pore complexity

In addition, the extracted pore geometry characteristics are employed to calculate the pore complexity of each image. The roundness and elongation of pores are used as inputs of the following equation [28]:

$$\text{PoreComplexity} = \left(\frac{7}{22.14} \times \text{roundness}\right) + \left(\frac{3}{7.65} \times \text{elongation}\right) \quad (1)$$

The mean value of pore complexity of all studied pore spaces is considered as the image pore complexity, which is used as an input for the classifier models. The pore complexity value ranges from 1 to 10 theoretically for the simple and complex pores, respectively. In Eq. 1, the numbers 7 and 3 prescribe the contribution of roundness and elongation in the complexity of pores. The weight of roundness is considered larger as its variations have larger effects on the geometrical complexity of pores. 22.4 and 7.65 are the maximum roundness and elongation, respectively, among all the studied pore spaces. These values may differ for another case study.

4.3. Cement percentage

The cementation performs the role of a permeability destructive factor in heterogeneous carbonates. The main type of cement in the

Kangan and Dalan formations is anhydrite and calcite. Both types of cements are white, and they are easily distinguishable in the images. Therefore, a simple point counting procedure on gray scale images is used to calculate the total percentage of cement in the thin section images. A try-and-error examination shows that in the gray scale images, all pixel values greater than 165 can be considered as cement. The intensity histogram of images is shown in Figure 5.

Studying the thin sections shows that the cement growth affects the permeability by plugging the pore throat. Figure 6 illustrates some samples with a high percentage of cement growth. In spite of fair porosity, the permeability is dramatically reduced by the cement growth. The cement pixels were highlighted in the right-side images by white color. In Figure 6a, the the rock matrix was gradually converted to cement, while the cement was filled some oolitic pores ($\phi = 8.7\%$ and $K = 0.6$ mD). Figure 6b shows that cementation mostly happens in grains. Both the isolated pores and cementation cause a low permeability in spite of a high porosity ($\phi = 14.1\%$ and $K = 1.6$ mD). Figure 6c is an example of the destructive cement growth in all possible interparticle pore spaces, which convert the porosity to non-effective because throats and pore connections are plugged by the cement ($\phi = 22.8\%$ and $K = 0.6$ mD).

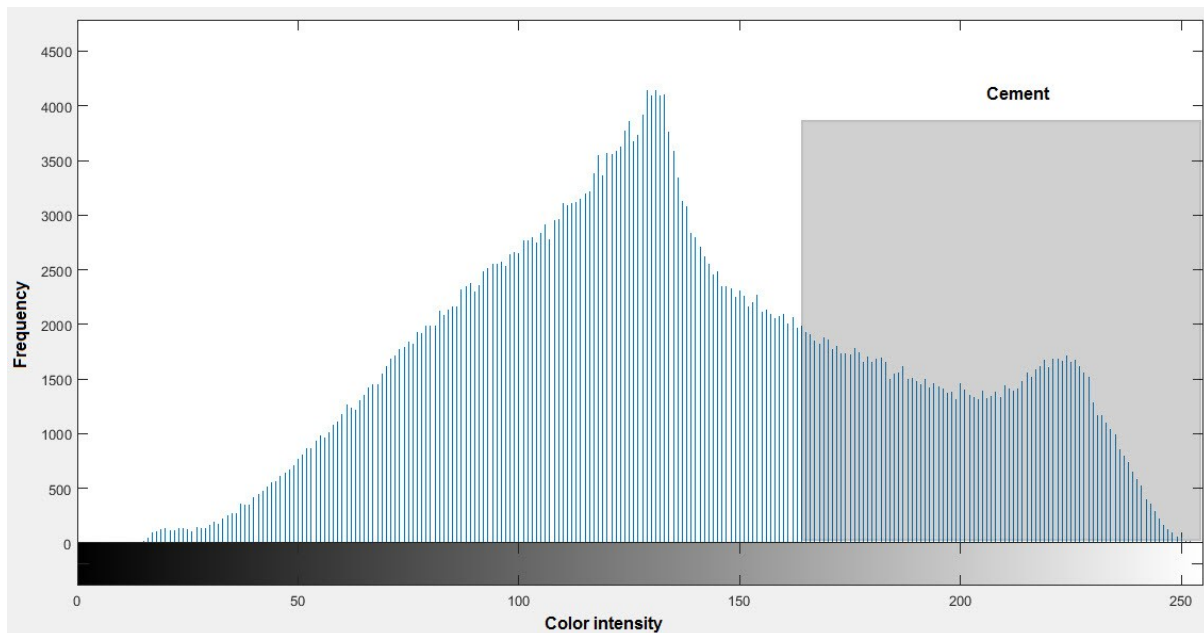


Figure 5. The intensity histogram for cement pixels indicating that the pixel values bigger than 165 belong to cement pixels.

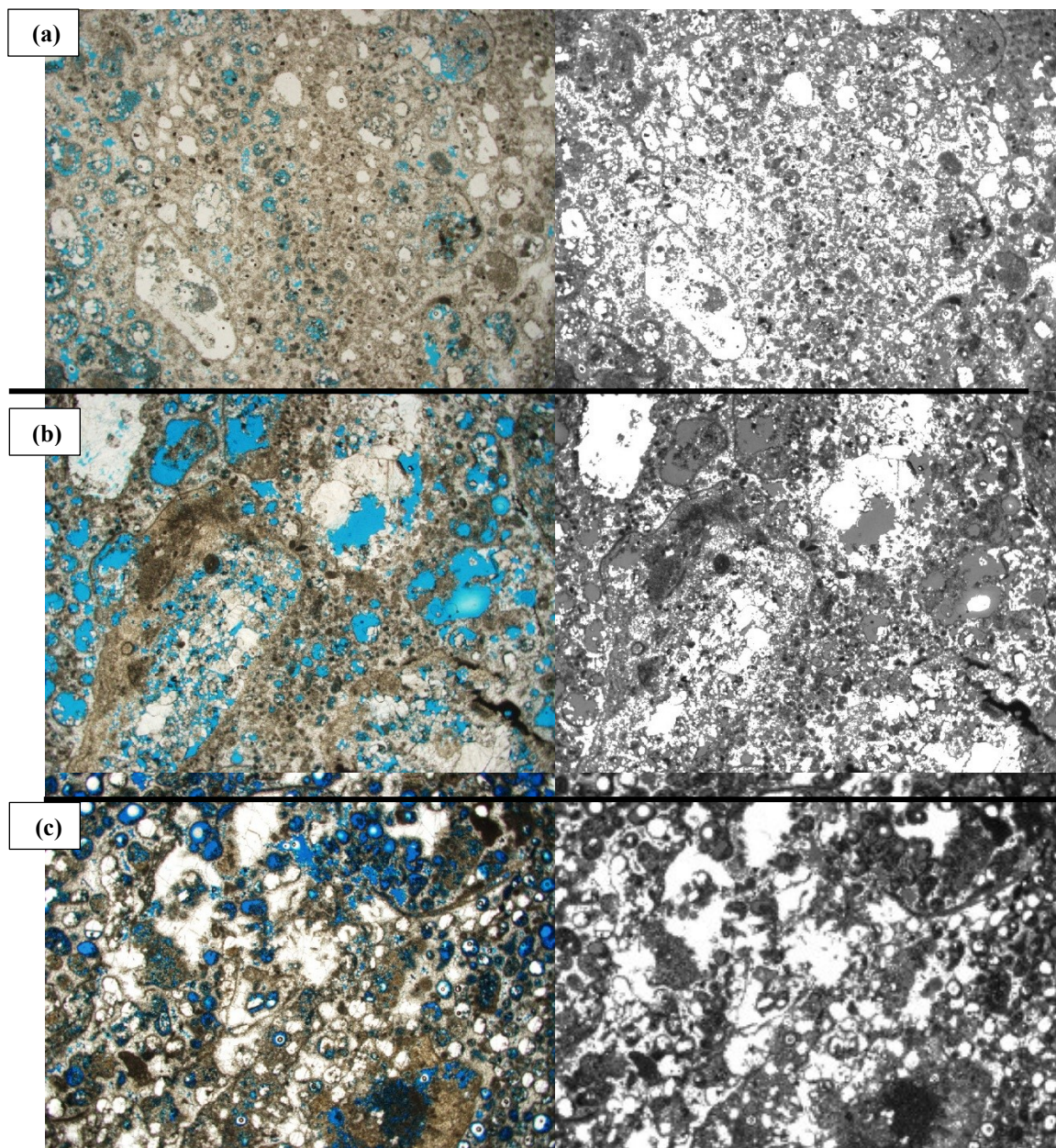


Figure 6. Three samples with extensive cement growth in the porous media (a) cement growth in the oolitic pores, (b) cementation in the rock matrix and grains, and (c) destructive cement growth in the interparticle pores and throats.

4.4. Textural characteristics

The studied images were classified into four categories including mudstone, wackstone, packstone, and grainstone based on the Dunham classification [29]. Figure 7 shows the distribution of each texture type in the permeability classes. All samples of class#1, less one, are mudstone, which means that contiguous mudstone facies is susceptible for a low permeable zone in Kangan and Dalan formations.

Figure 8 illustrates four types of samples with a grainstone texture, while the petro-physical properties are considerably different. A facies with a grainstone texture can be an excellent

reservoir zone if the post-depositional processes have not destroyed the petro-physical properties. Figure 8a shows an exception example, where a grainstone texture belongs to class#1, in which a high percentage of cement (37%) filled all the porous media and both porosity and permeability were completely destroyed ($\phi = 2\%$ and $K = 1$ mD). Figure 8b is another grainstone that belongs to class#2, in which the isolated moldic pore spaces provided high percentages of porosity but permeability was negligible because the pores were not connected ($\phi = 26.4\%$ and $K = 0.4$ mD). Figure 8c represents a grainstone of class#3 in which low sorting is obvious, and the calcite

cement somehow fills most of the interparticle pores ($\phi = 21\%$ and $K = 15.5$ mD). Finally, Figure 8d is a perfect case of carbonate texture in which both porosity and permeability are high and the

throats are not plugged. Such a situation grants the best reservoir quality for a rock ($\phi = 19\%$ and $K = 180$ mD). Cement growth was not widely filled with the pore spaces and pore throats.

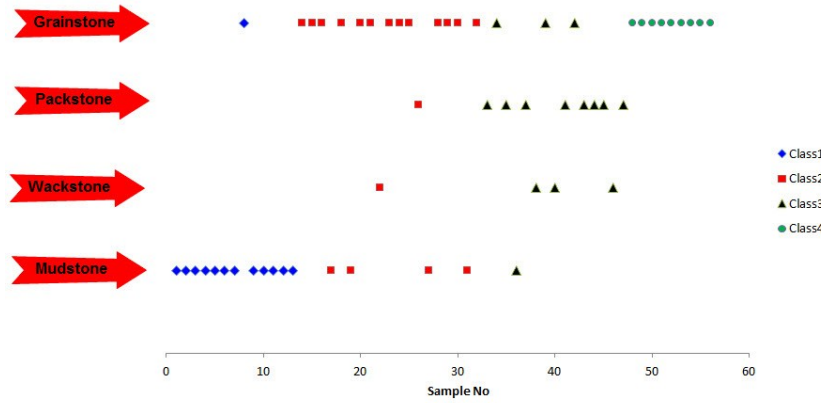


Figure 7. Frequency of Dunham texture in the defined classes of permeability in the studied limy formation.

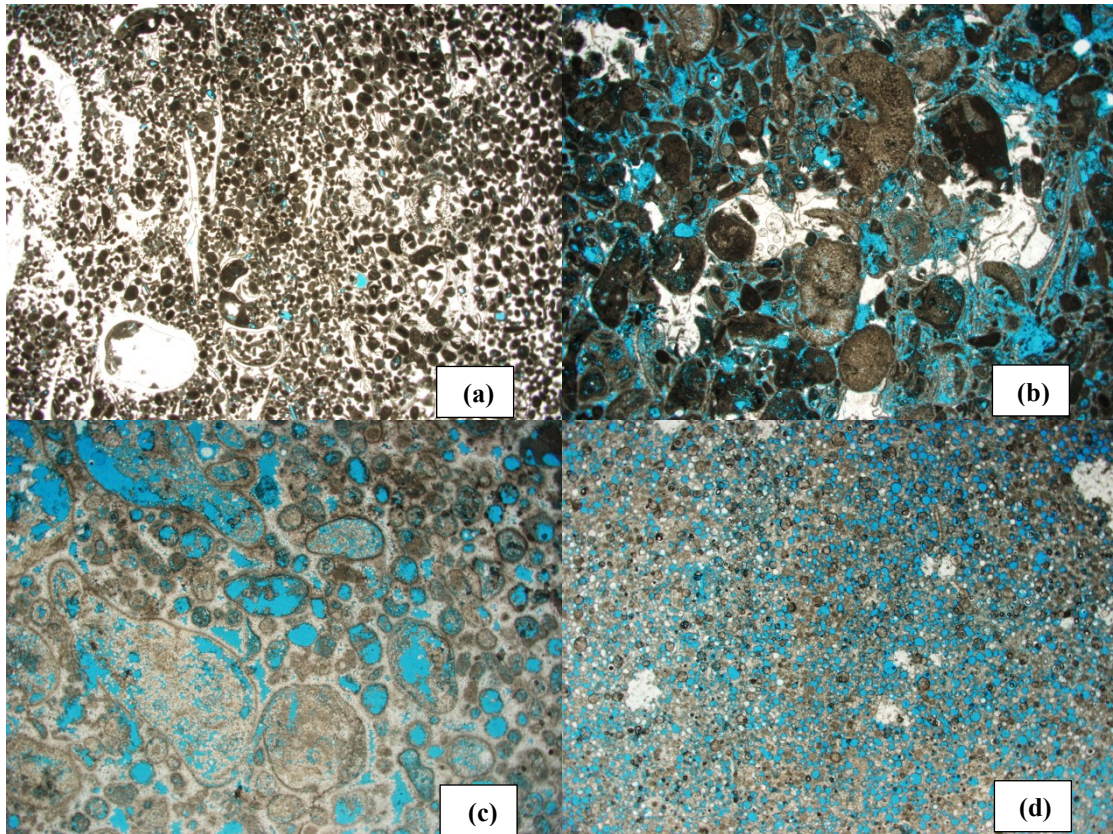


Figure 8. Four grainstone samples with different pore-physical characteristics belonging to (a) class#1, (b) class#2, (c) class #3, and (d) class#4.

The abundance of each type of porosity versus the texture type in the permeability classes is represented in Figure 9. The high abundance of interparticle porosity beside grainstone texture created a high quality reservoir rock, while the interparticle porosity ratio in class #1 and class#2 was negligible. In addition, grainstones of class#3

have moderate abundance of interparticle porosity (Figure 9a). The major abundance of moldic porosity was detected in grainstones of class #2, which meant that the moldic pores were isolated. The presence of high percentages of moldic pores in a grainstone texture does not improve the permeability (Figure 9b). On the other hand,

micro-porosity is the main porosity type in mudstone samples. As expected, the micro-pores have no positive effects on fluid flow inasmuch as it is dominant in class#1 samples (Figures 9d and 9e). The interparticle porosity was detected in all classes. Commonly, interparticle pores perform as a non-effective porosity in carbonates unless fractures connect them through the rock fabric (Figure 9c). The vuggy porosity is not abundant in the Kangan and Dalan formations, and some samples of class#2 show the presence of vug pores. There is no evidence that a low percentage of vug pores in class#2 samples promotes the pore connectivity (Figure 9f). The presence of interparticle pores directly affects the reservoir quality in the studied samples if the cementation process has not blocked the pore throats. The abundance of porosity types, total optical porosity, mean pore complexity, cement percentage, and textural characteristics of each image are extracted. The image-based data is annexed to the corresponding class. The training matrix of intelligent classifiers involves nine columns. The first nine columns are inputs including optical porosity, texture type, mean pore complexity, cement percentage, and abundance of interparticle, moldic, interparticle, vuggy, and microporosity. The last column represents the reservoir class, labeled as 1, 2, 3, and 4.

5. Materials and methods

Data mining is the process of efficient algorithm implementation for the exploitation of valuable information hidden in a set of data points. Working with a limited number of data points brings some uncertainties in the algorithms decision. In the present paper, the applications of various simple and ensemble data classifier algorithms including K-nearest neighbor (KNN) classifiers, support vector machines (SVM), discriminant analysis (DC), multi-layer perceptron (MLP), decision trees (DT), bagging, and boosting are addressed for reservoir classification. Two factors are considered for selecting the algorithm: first, their popularity among the researchers. Secondly, difference in the mathematical and statistical fundamentals, which helps to analyze the data from different viewpoints.

5.1. Discriminant analysis

A statistical machine-learning algorithm was employed for feature extraction, data reduction, and classification issues. The weight or coefficient factors of discriminant functions were calculated

using a training matrix. A set of discriminant functions were trained to assign the input array to one of the pre-defined categories based on the discriminant score of the functions. Then the unseen data was assigned to one class, which had the maximal discriminant score. The scores were defined in terms of posterior probability of belonging to each class [30]. The general form of discriminant function was derived as:

$$H_i(X) = -\frac{(X - \mu_i)^T \times (x - \mu_i)}{2 \sum_i} - \frac{n}{2} \times \ln(2\pi) - \frac{\ln|\sum_i|}{2} + \ln P(C_i) \quad (2)$$

Different types of discriminant functions including linear, quadratic, and mahalanobis were defined, which could be utilized based on the type and hierarchy of the training data. Details of the discriminant analysis can be found in [27].

5.2. Support vector machine

The algorithm is a supervised statistical data mining approach introduced for the first time by Cortes and Vapnik [31] for text recognition. A support vector machine classifies the data in three steps. First, the SVM maps the available training data as points in space. Then it uses a non-linear transform to convert the input vectors into a higher dimension space, and finally, it separates the categories by optimal linear hyperplane so that an obvious margin can be detectable between the data in two classes. More details about the SVM algorithms can be found in [32].

5.3. Decision tree algorithm

Decision trees are predictive algorithms adopting their name from their tree form structure. Three types of nodes are defined for a decision tree algorithm including decision, uncertainty, and leaf nodes, which are shown by circle, square, and triangle in the graphical flowchart, respectively. A classification path is started from the root, continued in the branches, and finally, ended to a leaves in which the class label is defined. The branches play the role of conjugations for the inputs and outputs. The decision rules for different conditions are defined using *if clauses*. In a decision tree, all possible scenarios of a problem are considered based on certain conditions transparently. The process of classification is observable in a white box model, which makes the classification procedure explicit. Comprehensive and transparent nature, and computational simplicity as well as easiness of application are

the advantages of the decision tree model. Three types of singular decision trees including simple, medium, and complex decision trees as well as

two ensemble types named boosted and bagged trees are employed for reservoir classification.

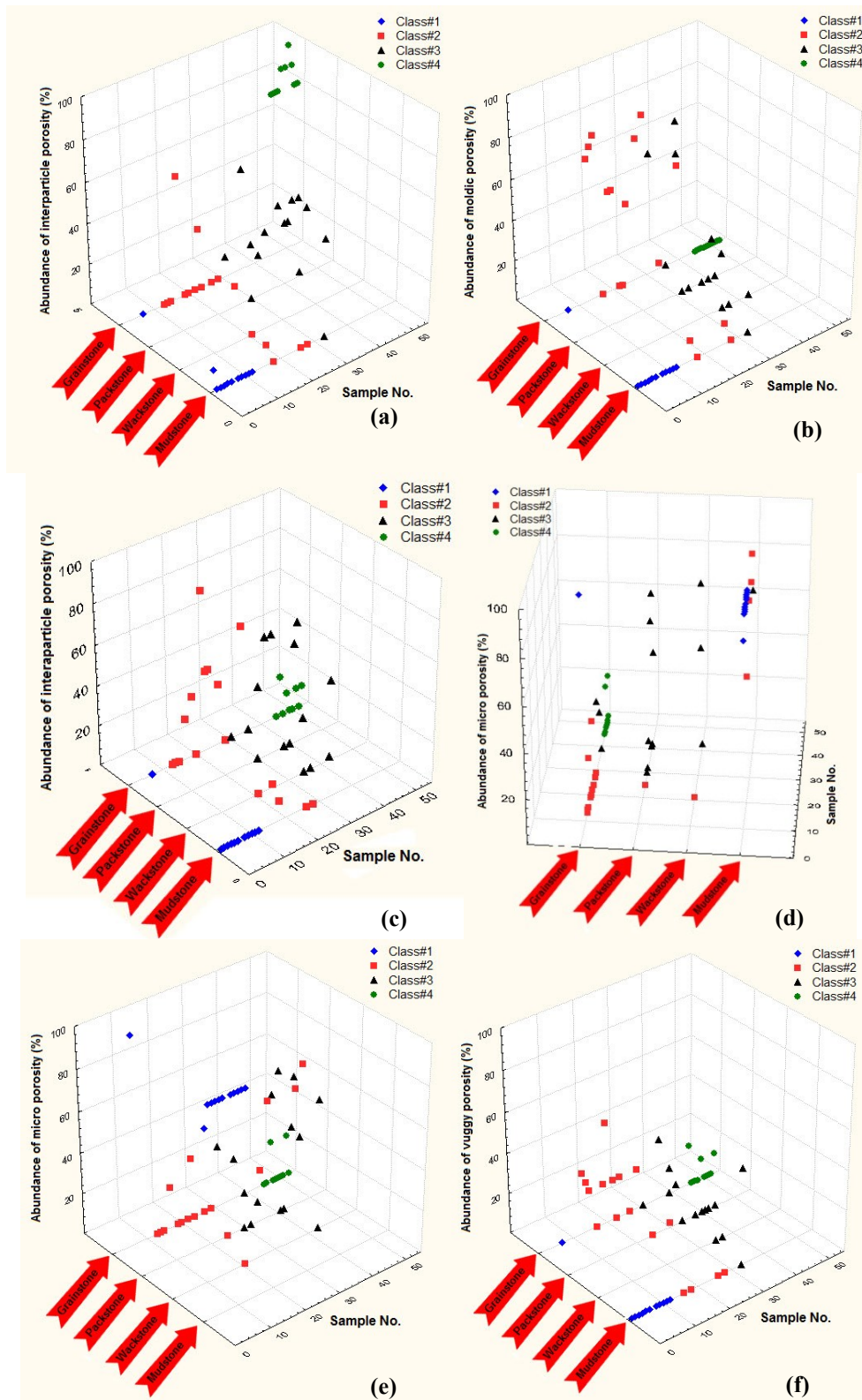


Figure 9. The abundance of (a) interparticle porosity, (b) moldic porosity, (c) interparticle porosity, (d) micro-porosity (side-view)(e) micro-porosity (top view), and (f) vuggy porosity versus the texture type in the studied samples.

5.4. K-nearest neighbor classifiers (KNN)

A simple and non-parametric approach was extensively employed in the classification proposed by Cover and Hart [33]. The present form of KNN is the modified version by Altman [34]. The data points are classified based on the desirable number of categories defined by the user and the most similar instances of the input points that consist of the *k* closest training examples in the *feature space*. The *k* number defines the number of neighbors influencing the classification. The instance similarity between the data points (*x_i*) and a fix point (*x*) is measured through a common distance metric such as Euclidean and Hamming for continues and discrete variables, respectively. The data is ranked based on the closeness to point *x*. The KNN classifier is also known as lazy learning algorithms insomuch it postpones all the necessary computations to the classification time. In the present work, different types of KNN classifiers named fine KNN, medium KNN, coarse KNN, cosine KNN, cubic KNN, and weighted KNN were trained and verified.

5.5. Ensemble methods

All the aforementioned classifiers benefit from some advantages and suffer from some inaccuracies in generalization of data points. This fact is more obvious when the number of data points is limited and the data complexity is high. The theoretical studies and practical experiences suggest that there is no *best* methodology for all classification problems. The respective distribution of training data points applies a crucial impact on the accuracy of the utilized classifier. If the respective distribution in each class of data is normal, then discriminant analysis performs accurate, and if not, other methods such as Kernel-based SVM and KNN perform better. Integrating multiple classifiers may improve the generalization and stability of single algorithms. In the current work, two ensemble strategies named bagging and boosting were used to improve the results and reduce the variance of singular algorithms. Both strategies integrate a group of weak classifiers to generate a more accurate model that performs better and more stable. In an ensemble approach, several models are trained based on the same learning algorithm, and then the results are fused to obtain the final output more accurate.

5.5.1. Bagging

The bagging strategy, also called bootstrap aggregation, was introduced by Breiman [35]. This method employs a learning method, and it has been applied to several statistically similar sets of training data. Three steps are necessary to develop a bagged classifier. First, new sets of training data are generated by random sampling with replacement from the original training data set. Then several single classifiers are trained using the new generated training datasets. Finally, a weight averaging is used to combine the obtained models. Although it is usual to implement this strategy for decision trees due to the high degree of instability of these algorithms, it can be utilized for other intelligent classifiers. The structure of decision trees can be thoroughly altered by small changes or modifications in training data points. The instability problem is easy to solve if several training datasets are available from a similar distribution. For each bootstrap training dataset, a singular classifier is trained, and then averages the results of singular models to reduce the instability effect.

5.5.2. Boosting

Boosting is another ensemble strategy employed for improving the results of singular classifiers proposed by Freund and Schapire [36]. Unlike bagging, the appearance probability of elements in the newly generated training datasets is unequal. The input vectors are weighted and some of them have a higher chance to contribute to the new sets. Two types of weights are defined in the boosting strategy: first, for adjusting the contribution of data points (*B_i*), and secondly, for integration of the singular classifiers (*W_j*), where *j* = 1, ..., *m*. At the beginning, the initial weight of all input vectors is equal (*B_i* = 1/*n*) for the given training data [*X_i*, *Y_i* | *i* = 1, 2... *n*], where *X_i* and *Y_i* are the input and output vectors, respectively. The singular classifiers (*C_j(x)*) are trained using the subsets of initial training data. The accuracy of single classifiers and their contribution weights (*W_j*) are calculated as below.

$$Accuracy_i = \frac{\sum_{i=1}^n B_i I(Y_i = C_j(x_i))}{\sum_{i=1}^n B_i} \tag{3}$$

$$\text{So that } \begin{cases} I(\text{false}) = 0 \\ I(\text{true}) = 1 \end{cases}$$

$$W_j = \log\left(\frac{Accuracy_i}{1 - Accuracy_i}\right) \quad (4)$$

The data point weight (B_i) is tuned in each iteration of the algorithm to increase the weight of misclassified data and clarify the effect of difficult cases for the classifier, as below.

$$B_i = B_i e^{(w_j I(Y_i \neq C_j(x_i)))}$$

So that $\begin{cases} I(false) = 0 \\ I(true) = 1 \end{cases} \quad (5)$

and $\begin{cases} i = 1, \dots, n \\ j = 1, \dots, m \end{cases}$

Then new subsets of training data are developed, and the single classifiers are trained. The cycle is repeated until the maximum predefined iteration of the user is reached. Finally, the ensemble classifier is obtained using a weighted averaging of the single classifiers:

$$EnsembleModel = \sum_{i=1}^m (w_i \times C_i(x)) \quad (6)$$

The contribution weight (W_i) of single classifiers depends on their performance and accuracy. The classifier with a higher accuracy and a lower error receives a larger weight and more contribution to the final decision.

5.6. Validation of classifiers

There are two well-known strategies of model verification, named K-fold and held-out. The held-out strategy was suggested for colossal dataset, while K-fold cross-validation is perfect when working with a limited number of data points (Yadav and Shukla [37]). The K-fold examination divides the training data into K subsets and then trains the classifier K times; each time, one of the subsets is used for validation. Finally, the mean values of K model accuracy is represented as the final accuracy of the classifier. The computational time of k-fold strategy is high, especially with a large value of K; however, in the present research work, the classifiers were evaluated using the K-fold cross-validation ($K = 10$). In addition, the performance of the classifiers was evaluated using four evaluation metrics, named accuracy, precision, recall, and harmonic average. The accuracy is the most general form of a metric to evaluate the overall performance.

$$Accuracy = \frac{1}{N} \sum_{i=1}^N I(\text{PredictedClass} = \text{ActualClass}) \quad (7)$$

So that $\begin{cases} I(false) = 0 \\ I(true) = 1 \end{cases}$

where N is the number of data points. Precision and recall are useful when dealing with imbalanced datasets, which separately represent the performance of the classifier for each category. The data was divided into two parts, named desired and undesired, to calculate the precision of each class. The desired group is generated from the samples of interest of the studied class classified correctly, while the undesired data includes samples of other classes misclassified as the studied class.

$$\text{Precision or Recall (Class}_i) = \frac{\text{Number of desired samples}}{\text{Number of desired} + \text{undesired samples}} \quad (8)$$

The formula of *Recall* is the same as precision, while the undesired data is defined as the samples of the class of interest misclassified as the other classes. Precision and recall can be generalized to the model by applying a weight averaging on the value of all classes. The weight value of each class is equal to the ratio of data population in the class to the total number of samples. Finally, the harmonic average of precision and recall is calculated using the following formula.

$$\text{Harmonic_average} = \frac{2 \times \text{Precision}(\text{class}_i) \times \text{Recall}(\text{class}_i)}{\text{Precision}(\text{class}_i) + \text{Recall}(\text{class}_i)} \quad (9)$$

6. Results and discussion

In the current section, the results of classification of algorithms for a real case study are reported. Not only the total model accuracy was considered for all classes but also precision and recall as well as harmonic average were calculated to analyze the performance of each class self-sufficiently. Table 3 represents the accuracy of all trained models through 10-fold cross-validation.

6.1. Overall accuracy evaluation

In this sub-section, the performance of the trained models was investigated in overall using the two concepts of accuracy and weighted harmonic average. Among the different decision tree models, the simple, medium, and complex trees were selected and trained. A Gini's diversity

index was used as the split criterion for all the models, while the maximum number of splits was 4, 20, and 100 for the simple, medium, and complex models, respectively. The simple decision tree with an accuracy of 86.3% had the best performance, which meant that increasing the number of splits had no effect on the model accuracy.

The performance of the linear and quadratic discriminant functions was very close, while the quadratic discriminant showed a higher accuracy (an accuracy of 87.2% and a harmonic average superior to 86.8%). Both models were regularized by diagonal covariance.

The support vector machine was another algorithm employed for the permeability classification. Various types of Kernel functions including linear, quadratic, cubic, fine Gaussian, medium Gaussian, and coarse Gaussian were employed to find a model with the best convergence. The box constraint level of the models was one. The only difference between the fine, medium, and coarse Gaussian Kernel function was the Kernel scale that was 0.71, 2.8, and 11 for fine, medium, and coarse, respectively. Among the SVM models, the linear Kernel function had the best convergence for permeability classification with an accuracy of 86.3% and a harmonic average of 86.9%.

Five types of KNN models, named fine, medium, coarse, cubic, and weighted, were trained. The number of neighbors for the fine, medium, and coarse models was 1, 10, and 100, respectively, while the distance metric was Euclidean for all the three models. The number of neighbors for both the cubic and cosine models was 10, while the distance metric was cosine and Minkowski, respectively. The distance weight of all aforementioned KNN models was equal. The last model was weighted KNN with 10 neighbors, and the Euclidean distance in which the distance weight was squared invers. The medium KNN was the best, while the accuracy of the coarse KNN model was dramatically low. Increasing the number of neighbors caused many misclassifications, and all samples of class #3 and class#4 were wrongly classified.

Finally, the performance of the two ensemble models was evaluated based on the theories of bagging and boosting. The accuracies of bagging and boosting were 91.3 and 94.9, respectively. The harmonic averages being 91.1 and 94.7 for bagging and boosting, respectively, also

confirmed the model performances. As expected, the ensemble models represent reliable results, and improve the accuracy of permeability classification up to 7.7% compared with the best single classifier.

6.2. Single class evaluation analysis

The overall evaluation results indicated that the intelligent classifiers were reliable considering all permeability classes. In this sub-section, the classifier performance was evaluated for each permeability class using the advantages of confusion matrix, which could be consequently employed to compute precision and recall. The medium decision tree, quadratic discriminant analysis, linear SVM, medium KNN, and bagged tree represented the best performance, each in its category, as shown in bold in Table 3; therefore, they were selected for per class evaluation using the advantages of confusion matrix. A confusion matrix is a square $n \times n$ matrix comparing the performance of the classifier, whereas the main diagonal elements denote the number of correct decisions. On the other hand, the value for element C_{ij} showed the samples of class i , which were misclassified as class j . Table 4 shows the confusion matrix of all aforementioned classifiers. The values for precision, recall, and harmonic average of each class were calculated through the confusion matrix. Finally, the weight average of precision and recall for each classifier was computed. Table 5 states that the best classification is obtained for class 4, in which all classifiers, except linear SVM, correctly classify all data points. The second rank belongs to class#1 so that three classifiers including QDA, linear SVM, and ensemble bagged tree recognized the correct class for all samples. The best precision of class#3 was 96.5%, which was obtained by the ensemble bagged tree, and then the medium KNN showed an accuracy of 92%. Unfortunately, the recall value of medium KNN for class#3 was 74.1%, which was 16.2% lower than the recall value of ensemble bagged tree. The ensemble bagged tree performed better than all models for class#3 permeability prediction considering the precision and recall values for all models. The last but not the least rank belongs to class#2, in which the precision and recall values are smaller compared to the other permeability classes. Overall, the ensemble-bagged tree presented the best classification of permeability using the petrographic and image analysis data.

Table 3. The accuracy and harmonic average of all trained classifiers for permeability classification.

Algorithm	Type of Classifier	Evaluation metrics	
		Accuracy (%)	Harmonic average (%)
Decision Tree	Complex Tree	85.5	85.2
	Simple Tree	86.3	86.1
	Medium Tree	85.5	85.2
Discriminant Analysis	Linear Discriminant	86.3	85.9
	Quadratic Discriminant	87.2	86.8
SVM	Linear SVM	87.2	86.9
	Quadratic SVM	85.5	85.6
	Cubic SVM	84.6	84.9
	Fine SVM	65.8	66
	Medium SVM	86.2	86.1
	Coarse SVM	84.6	84.3
	Medium KNN	86.3	85.9
KNN	Coarse KNN	39.3	27
	Cubic KNN	85.5	85.2
	Cosine KNN	81.2	80.3
	Weighted KNN	85.5	85.2
Ensemble	Ensemble Boosted Tree	91.3	91.1
	Ensemble Bagged Tree	94.9	94.7

Table 4. The confusion matrix of five classifiers with the best performance each within its category.

Actual Class	Predicted Class																			
	Simple tree				QDA				Linear SVM				Medium KNN				Ensemble Bagged			
	1	2	3	4	1	2	3	4	1	2	3	4	1	2	3	4	1	2	3	4
1	34	2	0	0	36	0	0	0	36	0	0	0	35	1	0	0	36	0	0	0
2	4	26	4	0	4	27	3	0	4	26	4	0	5	26	2	1	2	31	1	0
3	0	4	25	2	7	1	23	0	1	5	25	0	2	5	23	1	0	2	28	1
4	0	0	0	16	0	0	0	16	0	0	1	15	0	0	0	16	0	0	0	16

Table 5. The precision and recall of five classifiers with the best performance each within its category.

Permeability Class	Evaluation Metrics									
	Simple tree		QDA		Linear SVM		Medium KNN		Ensemble Bagged	
	Pr (%)	Re (%)	Pr (%)	Re (%)	Pr (%)	Re (%)	Pr (%)	Re (%)	Pr (%)	Re (%)
1	89.5	94.4	90	100	87.8	100	83.7	100	94.7	100
2	81.2	76.4	79.4	79.4	83.8	76.4	83.8	76.4	93.9	91.1
3	86.2	80.6	88.4	74.1	83.3	80.6	92	74.1	96.5	90.3
4	88.8	100	94.1	100	100	93.7	88.8	100	94.1	100
Average	86.1	86.3	87	87.2	87.1	87.1	86.6	86.3	94.8	94.8

7. Conclusions

In spite of several literatures concerning the implementation of intelligent models for permeability estimation, the present research work differs from the previous ones as explained below. First, most of the previous research works focused on the prediction of continuous values of permeability using the conventional well log data, while the present article discussed the potentials of intelligent classifiers for classification of reservoir intervals considering not only the Darcy value but also their porosity percentage. In addition, we introduced the advantages and capability of thin section images for reservoir characterization and recognition of permeable zones of the Kangan and Dalan formations. A

graphical comparison among the predicted reservoir class using intelligent classifiers and those derived from core data is shown in Figure 10. Thickness of the studied interval was around 35 m. There is a full agreement between the core derived and the intelligent classifier predictions in 31 m. of the studied intervals, while the ensemble bagged tree performed better than the others did. Implementation of data mining algorithms for real cases of carbonates rocks includes many complexities due to high heterogeneity and variations of fluid movement in such rocks. Here, micro-scale data was extracted from thin sections and used for macro-scale reservoir characterization. In fact, the results obtained for each point were generalized to an interval depth

that should be considered heterogeneous. The present comparison was done based on the limited number of available data points. A higher number of data points leads to a higher resolution in the reservoir characterization.

Finally, it is worth mentioning that all the results of this research work are based on the data points available from the Kanagan and Dalan formations

from one well of South Pars Gas Field. Certainly, a generalized and universal model for the whole gas field requires an extended number of data points. In addition, the geological conclusions about the texture and diagenesis processes of the Kanag and Dalan formations may differ in other wells.

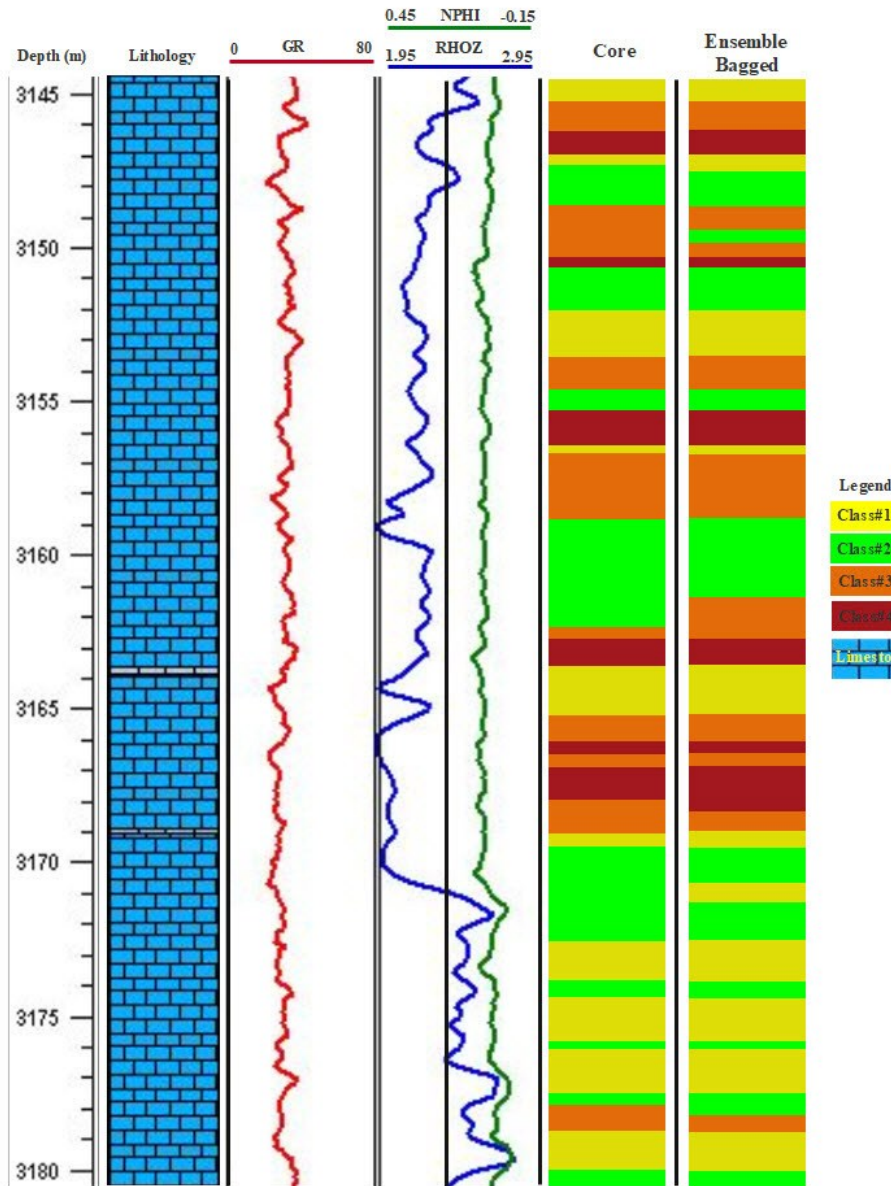


Figure 10. Image plot represents the predicted classes of reservoir quality using ensemble bagged and the measured classes based on core laboratory measurements. In the GR, NPHI, and RHOZ well logs, the lithology columns are attached to the reservoir characterization columns.

Acknowledgment

The Authors would like to appreciate Shahrood University of Technology (SUT) for providing the technical supports during this research. We also extend our appreciation to Dr. Sadeghiani from geology department of Shahrood University of

Technology for helping us during preparation of thin section images. In addition, helpful revisions and suggestions of two anonymous referees of Journal of Mining and Environment are kindly acknowledged.

References

- [1]. Saggaf, M.M. and Nebrija, L. (2003). Estimation of missing logs by regularized neural networks, AAPG Bulletin. (87): 1377-1389.
- [2]. Jamialahmadi, M. and Javadpour, F.G. (1999). Relationship of permeability, porosity and depth using an artificial neural network. J. Pet. Sci. Eng. 26: 235-239.
- [3]. Lim, J. (2005). Reservoir properties determination using fuzzy logic and neural network from well log data in offshore Korea. J. Pet. Sci. Eng. 49: 182-192.
- [4]. Saemi, M., Ahmadi, M. and Yazdian Varjani, A. (2007). Design of neural networks using genetic algorithm for the permeability estimation of the reservoir. Journal of Petroleum Science and Engineering. 59: 97-105.
- [5]. Qi, L. and Carr, T.R. (2006). Neural network prediction of carbonate lithofacies from well logs, Big Bow and Sand Arroyo Creek fields, Southwest Kansas. Computers & Geosciences. 32: 947-964.
- [6]. Anifowose, F. and Abdulaheem, A. (2011). Fuzzy logic-driven and SVM-driven hybrid computational intelligence models applied to oil and gas reservoir characterization. Journal of Natural Gas Science and Engineering. 3: 505-517.
- [7]. El-Sebakhya, E.A., Asparouhova, O., Abdulaheemb, A., Al-Majedb, A., Wua, D., Latinskia, K. and Raharja, I. (2012). Functional networks as a new data mining predictive paradigm to predict permeability in a carbonate reservoir. Expert Systems with Applications. 39: 10359-10375.
- [8]. Zargari, H., Poordad, S. and Kharrat, R. (2013). Porosity and Permeability Prediction Based on Computational Intelligences as Artificial Neural Networks (ANNs) and Adaptive Neuro-Fuzzy Inference Systems (ANFIS) in Southern Carbonate Reservoir of Iran. Journal Petroleum Science and Technology. 31: 1066-1077.
- [9]. Anifowose, F.A., Labadin, J. and Abdulaheem, A. (2014). Non-linear feature selection-based hybrid computational intelligence models for improved natural gas reservoir characterization. Journal of Natural Gas Science and Engineering. 21: 397-410.
- [10]. Jamshidian, M., Hadian, M., Mansouri Zadeh, M., Kazempoor, Z. and Salehi, H. (2015). Prediction of free flowing porosity and permeability based on conventional well logging data using artificial neural networks optimized by Imperialist competitive algorithm- A case study in the South Pars gas field. Journal of Natural Gas Science and Engineering. 24: 89-98.
- [11]. Karimpouli, S., Fathianpour, N. and Roohi, J. (2010). A new approach to improve neural networks' algorithm in permeability prediction of petroleum reservoirs using supervised committee machine neural network (SCMNN). Petroleum Science and Engineering. 73: 227-232.
- [12]. Jafari, S.A., Mashohor, S. and Jalali Varnamkhasti, M. (2011). Committee neural networks with fuzzy genetic algorithm. Journal of Petroleum Science and Engineering, 76: 217-223.
- [13]. Jafari Kenari, A. and Mashohor, S. (2013). Robust committee machine for water saturation prediction. Journal of Petroleum Science and Engineering. 104: 1-10.
- [14]. Golsanami, N., Kadkhodaie-Ilkhchi, A., Sharghi, Y. and Zeinali, M. (2014). Estimating NMR T2 distribution data from well log data with the use of a committee machine approach: A case study from the Asmari formation in the Zagros Basin, Iran. Journal of Petroleum Science and Engineering. 114: 38-51.
- [15]. Nourafkan, A. and Kadkhodaie-Ilkhchi, A. (2015). Shear wave velocity estimation from conventional well log data by using a hybrid ant colony- fuzzy inference system: A case study from Cheshmeh-Khosh oilfield. Journal of Petroleum Science and Engineering. 127: 459-468.
- [16]. Anifowose, F.A., Labadin, J. and Abdulaheem, A. (2017). Ensemble machine learning: An untapped modeling paradigm for petroleum reservoir characterization. Journal of Petroleum Science and Engineering. 151: 480-487.
- [17]. Cranganu, C. (2007). Using Artificial Neural Networks to Predict the Presence of Overpressured Zones in the Anadarko Basin, Oklahoma. Pure appl. geophys. 164: 2067-2081.
- [18]. Aydin, A. (2004). Fuzzy set approaches to classification of rock masses. Engineering Geology. 74: 227-245.
- [19]. El Ouahed, A.K., Tiab, D. and Mazouzi, A. (2005). Application of artificial intelligence to characterize naturally fractured zones in Hassi Messaoud Oil Field, Algeria. Journal of Petroleum Science and Engineering. 49 (4): 122-141.
- [20]. Dubois, M.K., Bohling, G.C. and Chakrabarti, S. (2007). Comparison of four approaches to a rock facies classification problem. Computers & Geosciences. 33: 599-617.
- [21]. Hu, J., Zhang, L., Liang, W. and Wang, Z. (2009). Incipient mechanical fault detection based on multifractal and MTS methods. Petroleum Science. 6: 208-216.
- [22]. Al-Bulushi, N., King, P.R., Blunt, M.J. and Kraaijveld, M. (2009). Development of artificial neural network models for predicting water saturation and fluid distribution. Journal of Petroleum Science and Engineering. 68: 197-208.
- [23]. Kamyab, M.R., Sampaio, H.B., Qanbari, F. and Eustes, A.W. (2010). Using artificial neural networks

to estimate the z-factor for natural hydrocarbon gases. *Journal of Petroleum Science and Engineering*. 73: 248-257.

[24]. Sharma, L.K., Vishal, V. and Singh, T.N. (2017). Predicting CO₂ permeability of bituminous coal using statistical and adaptive neuro-fuzzy analysis. *Journal of Natural Gas Science and Engineering*. 42: 216-225.

[25]. Hatampour, A., Schaffie, M. and Jafari, S. (2017). Estimation of NMR Total and Free Fluid Porosity from Seismic Attributes Using Intelligent Systems: A Case Study from an Iranian Carbonate Gas Reservoir. *Arabian Journal for Science and Engineering*. 42: 315-326.

[26]. Elkatatny, S. and Mahmoud, M. (2017). Development of a New Correlation for Bubble Point Pressure in Oil Reservoirs Using Artificial Intelligent Technique. *Arabian Journal for Science and Engineering*. 43 (5): 1-10.

[27]. Ghiasi-Freez, J., Soleymanpour, I., Kadkhodaie-Ilkhchi, A., Ziiai, M. and Hatampour, A. (2012). Semi-automated Porosity Identification from Thin Section Images Using Image Analysis and Intelligent Discriminant Classifiers. *Journal of Computers & Geosciences*. 45: 36-45.

[28]. Tonietto, S.N., Smoot, M.Z. and Pope, M. (2014). Pore Type Characterization and Classification in Carbonate Reservoirs. Poster presentation given at AAPG Annual Convention and Exhibition, Houston, Texas, April 6-9.

[29]. Dunham, R.L. (1962). Classification of carbonate rocks according to their depositional texture. In: Ham, W.E. (Ed.), *Classification of Carbonate Rocks-A Symposium*. American Association of Petroleum Geologists Memoir, Tulsa. pp. 108-121.

[30]. Hastie, T., Tibshirani, R. and Friedman, J. (2001). *The elements of statistical learning*, Springer Series in Statistics. Springer.

[31]. Cortes, C. and Vapnik, V. (1995). Support-Vector Networks. *Machine Learning*. 20 (3): 273-297.

[32]. Steinwart, I. and Christmann, A. (2008). *Support Vector Machines*. Springer New York. 601 P.

[33]. Cover, T. and Hart, P. (1967). Nearest neighbor pattern classification. *IEEE Transactions on Information Theory*. 13 (1): 21-27.

[34]. Altman, N.S. (1992). An introduction to kernel and nearest-neighbor nonparametric regression. *The American Statistician*. 46 (3): 175-185.

[35]. Breiman, L. (1996). Bagging Predictors. *Machine Learning*. 24 (2): 123-140.

[36]. Freund, Y. and Schapire, R.E. (1996). Experiments with a new boosting algorithm. In *Machine Learning: Proceedings of the Thirteenth International Conference*. pp. 148-156.

[37]. Yadav, S. and Shukla, S. (2016). Analysis of k-Fold Cross-Validation over Hold-Out Validation on Colossal Datasets for Quality Classification. *IEEE 6th International Conference on Advanced Computing (IACC)*.

بهبود دقت در طبقه‌بندی سنگ مخزن کربناته هتروژن با استفاده از استراتژی‌های تقویت کردن و بسته‌بندی: مطالعه موردی در کربنات‌های تریاس پایینی فارس ساحلی، جنوب ایران

جواد قیاسی فریز^{۱*}، منصور ضیائی^۱ و علی مرادزاده^۲

۱- دانشکده مهندسی معدن، نفت و ژئوفیزیک، دانشگاه صنعتی شاهرود، ایران

۲- دانشکده مهندسی معدن، دانشگاه تهران، ایران

ارسال ۲۰۱۸/۱/۲۷، پذیرش ۲۰۱۸/۵/۱۴

* نویسنده مسئول مکاتبات: javadghiasi86@gmail.com

چکیده:

ارزیابی دقیق مخزنی یکی از مهم‌ترین مؤلفه‌های لازم برای ایجاد مدل‌های کمی زمین‌شناسی و شبیه‌سازی مخزنی است. در پژوهش حاضر، یک نگاه جدید برای ارزیابی مخزنی ارائه شده که در آن از مزایای آنالیز تصویر مقاطع نازک و الگوریتم‌های طبقه‌بندی داده استفاده شده است. روش ارائه شده متشکل از سه مرحله اصلی است. در مرحله اول، بر پایه تعداد محدود اطلاعات تخلخل و تراوایی به دست آمده از آنالیز مغزه سازندهای کنگان و دالان، چهار کلاس مجزا برای سنگ مخزن کربناته تعریف شده است. سپس هفت شاخص میکروسکوپی تصاویر مقاطع نازک مشتمل بر توزیع فضاهای بین دانه‌ای، درون دانه‌ای، قالبی و حفره‌ای، پیچیدگی هندسی فضاهای خالی، توزیع سیمان و شاخصه‌های بافتی استخراج شده است. در مرحله آخر، شاخصه‌های استخراج شده از تصاویر با کلاس متناظر مخزنی به عنوان داده‌های آموزشی الگوریتم‌های طبقه‌بندی نظیر درخت تصمیم‌گیری، تابع آنالیز تفکیک کننده، ماشین بردار پشتیبان، مدل نزدیک‌ترین همسایگی و دو الگوریتم ترکیبی، به نام‌های تقویت کننده و بسته‌بندی، استفاده شده است. ارتباط بین مشخصه‌های میکروسکوپی و کلاس‌های مخزنی مورد بررسی قرار گرفت. عملکرد مدل‌های طبقه‌بندی با در نظر گرفتن مفاهیم دقت، صحت، فراخوانی و میانگین هماهنگ ارزیابی شده است. نتایج نشان می‌دهد روش بسته‌بندی درخت تصمیم‌گیری بهترین عملکرد را در میان مدل‌های مختلف داشته است و دقت طبقه‌بندی را در مقایسه با بهترین مدل ساده تا ۷/۷٪ بهبود داده است.

کلمات کلیدی: ارزیابی سنگ مخزن، روش‌های طبقه‌بندی هوشمند، استراتژی‌های تقویت کننده و بسته‌بندی، آنالیز تصویر مقاطع نازک، سازندهای کنگان و دالان.
